# Detection of an impact-generated dust cloud around Ganymede

**Harald Krüger*, Alexander V. Krivov†, Douglas P. Hamilton‡ & Eberhard Grün***

** Max-Planck-Institut für Kernphysik, Postfach 103980, 69029 Heidelberg, Germany*

*† Astronomical Institute, St Petersburg University, 198904 St Petersburg, Russia*

*‡ University of Maryland, College Park, Maryland 20742-2421, USA*

**Dust pervades the Solar System, and is concentrated in the ring systems surrounding the giant planets and along the plane of the planetary orbits (the Zodiacal cloud). Individual dust grains are thought to be generated when impacts loft material from larger bodies[20,21,23–27], such as satellites. Uncertainties in theoretical models of this ejection process are large, and there have hitherto been no direct measurements with which to constrain these models. Here we report *in situ* measurements of submicrometre dust within a few radii of Jupiter's satellite Ganymede. The directions, speeds and distribution of masses of the grains indicate that they come from Ganymede, and are consistent with an ejection process resulting from hypervelocity impacts of interplanetary dust onto Ganymede's surface. Dust appears also to be concentrated near Callisto and Europa, suggesting that these satellites too are significant sources of dusty debris.**

The Galileo spacecraft, orbiting Jupiter since 7 December 1995, is equipped with an impact ionization dust detector[1,2], which measures the plasma cloud released on impact of submicrometre and micrometre dust particles onto its sensor. Masses and impact speeds of the grains are determined from the measured amplitudes and rise times of the impact charge signals in three channels[3]. Each impact event is classified into one of four quality classes, with class 3 being dust impacts and class 0 being noise. Depending on the noise rate of the charge measurements on the individual channels, classes 1 and 2 can be true dust impacts or noise events[3,4]. As class 2 events were relatively noise-free during the Ganymede fly-bys, here we analyse the combined class 2 and class 3 data set.

During close fly-bys of the galilean moons, the overall impact rate of dust grains measured by the dust sensor showed a sharp peak within about half an hour centred on closest approach to each satellite[5–7]. Concentrations of dust were observed for Europa, Ganymede and Callisto, with the Ganymede data set being the most complete; during the combined primary and Galileo Europa Mission (GEM), Galileo had four close fly-bys at Ganymede, and no further encounters with this satellite are planned in the future. The times of the Ganymede fly-bys are given in Table 1, and the geometry of the Galileo dust detections is explained in Fig. 1.

The direction in which the sensor was pointing during dust impacts (rotation angle, $\Theta$) at the Ganymede encounters is shown in Fig. 2. During the first three encounters (G1, G2 and G7) particles with $180° \leqslant \Theta < 360°$ were detected at altitudes below $4R_G$ (Ganymede radius, $R_G = 2{,}635$ km) and were concentrated towards Ganymede. Particles recorded from the opposite direction ($0° \leqslant \Theta < 180°$) did not show such a concentration[6].

Analysis of the velocity vector of Ganymede relative to Galileo, taking into account the 140° field of view of the dust detector[1], shows that particles belonging to a dust cloud around Ganymede could be detected with $\Theta = 270 \pm 90°$ during all four encounters. Thus particles with $180° \lesssim \Theta \lesssim 360°$ detected during the first three fly-bys are compatible with having a Ganymede origin. We will call them Ganymede particles. Particles detected from the opposite direction ($0° \leqslant \Theta < 180°$) are streams of 10-nm dust grains[8,9] which probably originate from Io (refs 6, 7, and A. L. Graps *et al.*, manuscript in preparation). They are not considered here.

We have identified 35 Ganymede particles from the first three encounters purely by their impact direction (Table 1). The measured impact speeds of most Ganymede particles from these encounters

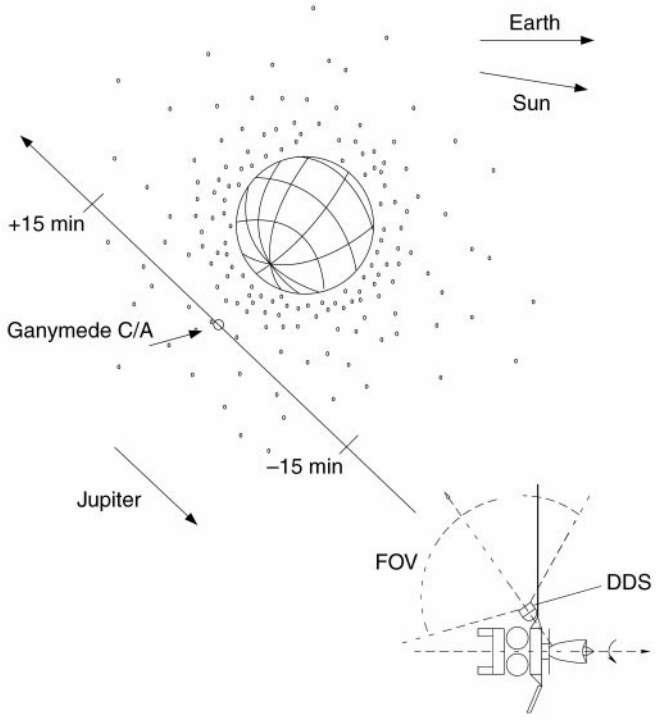


**Figure 1** Galileo's trajectory and geometry of dust detection during the G7 Ganymede fly-by. The Galileo spacecraft is sketched in an orientation it was in during the fly-by: the antenna points towards Earth and the dust detector scans the opposite hemisphere away from the Earth. The dust detector (DDS) has a conical field of view (FOV) of 140° and is mounted at an angle of 60° with respect to the positive spin-axis (anti-Earth direction). As Galileo spins about the spacecraft–Earth line, the dust detector axis sweeps out a cone with 120° opening angle, sampling dust arriving from different directions. The dust detector is shown here in an orientation where particles belonging to a cloud of dust from Ganymede can be detected (rotation angle $\Theta \approx 270°$). Dust-stream particles approach from the opposite direction (Jupiter direction, $\Theta \approx 90°$). C/A, closest approach.

**Table 1 Satellite encounter characteristics and dust impact detections**

| Fly-by | Time of C/A (year-day) | Altitude at C/A (km) | Particles with full data set | Corrected number of particles |
|---|---|---|---|---|
| G1 | 96-179.270 | 844 | 15 | 30 |
| G2 | 96-250.791 | 262 | 9 | 48 |
| G7 | 97-095.299 | 3,095 | 11 | 11 |
| G8 | 97-127.665 | 1,596 | 9* | 49 |

Galileo satellite fly-bys (first column) are labelled with the first letter of the galilean satellite which was the encounter target during that orbit, followed by the orbit number. C/A, closest approach. Galileo's data transmission capability is very limited because its high-gain antenna failed to open completely. Although each impact event is counted, the full set of measured parameters (such as impact direction, impact charge, and charge rise times) is not always transmitted to Earth. During the satellite encounters, the transmission rate was roughly one full impact parameter set per minute. The higher impact rates experienced during the G1, G2 and G8 encounters resulted in loss of some data. Because all impacts were counted, however, we can derive the true number of Ganymede particles (column 5) by multiplying the total number of impacts (from all directions) by the fraction of Ganymede particles for which we have full data sets (column 4)[10].

* Only particles with impact speed $v \leqslant 10\,\mathrm{km\,s^{-1}}$ and below $5R_G$ altitude included.

are below 10 km s$^{-1}$ with a mean value of 7.0 ± 4.8 km s$^{-1}$ (ref. 10). The stream particles, by contrast, have typical impact speeds (derived from the instrument's calibration) which are much higher than 10 km s$^{-1}$. Although the instrument calibration probably significantly underestimates the true speeds of the tiny dust-stream particles[11], the calibrated impact speeds can be used to distinguish Ganymede particles from the dust streams (Fig. 2, bottom panel). The measured impact speeds of Ganymede particles agree well with the expected impact speeds for debris moving with Ganymede, ~8 km s$^{-1}$ for all encounters, which suggests that these grains do indeed originate from Ganymede.

During Galileo's fourth Ganymede fly-by (G8), both dust streams and Ganymede particles approached the sensor from the same direction ($180° \leq \Theta < 360°$). On the basis of data from the first three encounters, we adopt two criteria to distinguish Ganymede particles from dust streams: (1) Ganymede particles must be within $5R_G$ of the satellite, and (2) the measured impact speed must be <10 km s$^{-1}$. Nine particles satisfy these criteria (Table 1).

To characterize the dust cloud of Ganymede, we derived both mass and spatial distributions for the detected grains. The slope of the cumulative mass distribution for particles in the mass range $10^{-16}$ to $10^{-13}$ kg is $\alpha = 0.98 \pm 0.06$ (ref. 10). This is consistent with the typical slopes expected for ejecta ($0.5 \lesssim \alpha \lesssim 1.0$; refs 12, 13). The spatial distribution of the dust grains is shown in Fig. 3. During the first three encounters (G1, G2 and G7) the number density increases towards Ganymede, with power-law slopes ranging between −0.43 and −2.85. For the G8 encounter, no concentration of particles towards Ganymede is seen, perhaps due to uncertainties imposed by the separation from the stream particles and the large correction for incomplete transmission. The concentration of dust towards Ganymede leaves no doubt that the satellite itself is the source, as its gravitational and electromagnetic forces are too weak to appreciably focus interplanetary and/or interstellar dust. Because there are no indications of geysers or volcanoes on Ganymede, the most likely source is the continuous ejection of debris via bombardment of Ganymede's surface by interplanetary micrometeroids.

In Fig. 3, we combine the data from all four Ganymede fly-bys on a single plot. In interpreting the plot, we assume that the flux of dust released from Ganymede is constant in time and is constant over the satellite's surface. These assumptions are probably not entirely true, but are accurate enough to allow simple order-of-magnitude estimates to be made. Most ejecta grains follow ballistic trajectories and strike Ganymede again within several hours to a few days. These short-lived but continuously replenished grains form a tenuous steady-state debris cloud which entirely envelopes Ganymede. Our measurements suggest a surprisingly large amount of orbiting ejecta

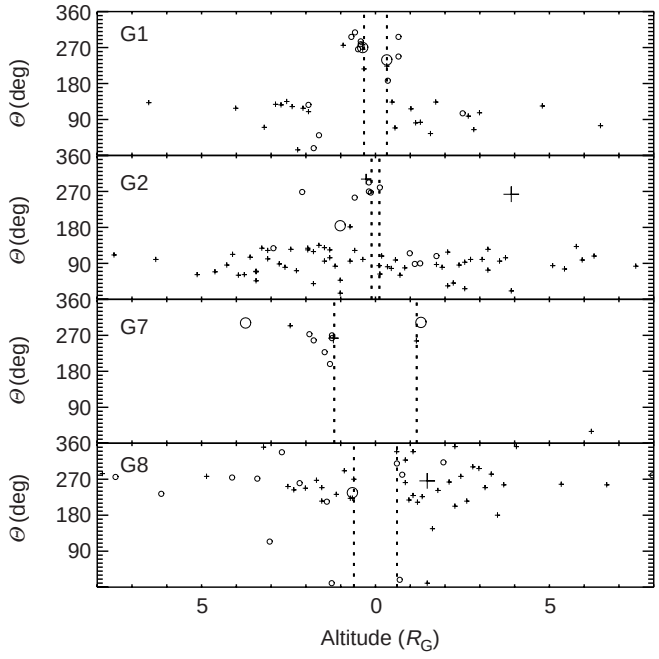


**Figure 2** Sensor direction (rotation angle, $\Theta$) versus altitude of the Galileo spacecraft above the surface of Ganymede at the time of dust impact. Data are shown for all four Ganymede encounters (G1, G2, G7, G8). The altitude range shown corresponds to a time interval of 1.6 h. At $\Theta = 0°$ the sensor axis points closest to ecliptic north, at 90° it points closest to the direction of Jupiter. The direction to Ganymede is ~270° during approach. Here we plot only impacts for which we have a complete set of parameters. The apparent concentration of these particles within $5R_G$ is due to an increased data transmission rate near Ganymede. Circles show particles with impact speeds below 10 km s$^{-1}$ and crosses show particles with higher speeds. The symbol sizes indicate the impact charge created by the particles ($10^{-14}$ C ≤ $Q_i$ ≤ $10^{-11}$ C). Ganymede's radius is $R_G$ = 2,635 km. Galileo did not pass through the altitude ranges between the dotted lines. For G1, G2 and G7, Ganymede particles approached from the opposite direction ($180 < \Theta \leq 360°$) to the stream particles ($0 < \Theta \leq 180°$). In G8, both types of particles approached from the same direction and they can be distinguished by their impact speed only.

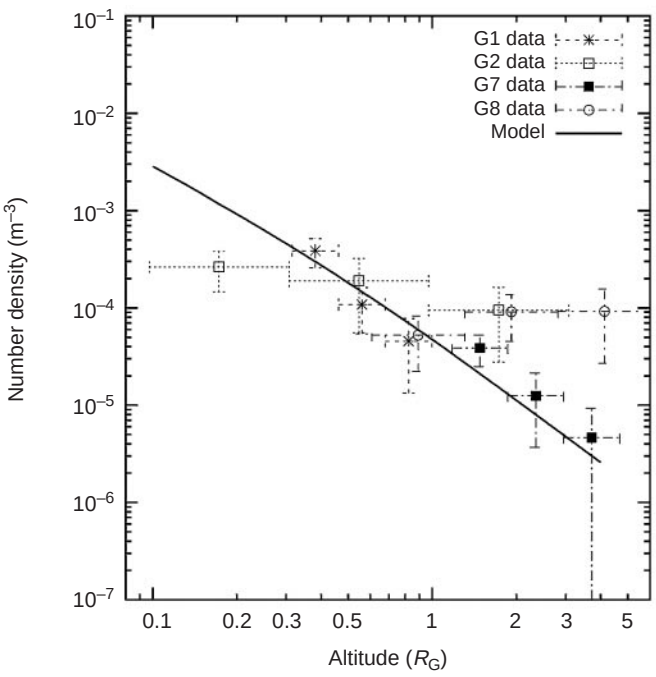


**Figure 3** The number density of dust as a function of altitude above the surface of Ganymede. To obtain the number density from the data (symbols with error bars), we first defined altitude ranges ('bins') equally spaced outwards from Ganymede on a logarithmic scale (indicated by horizontal bars). We then divided the number of particles for which the complete set of parameters has been transmitted to Earth in a given distance bin by the time Galileo has spent in this bin. We corrected for incomplete data transmission (Table 1) and divided the rates by the effective spin-averaged detector area to obtain fluxes (in m$^{-2}$ s$^{-1}$). Finally, we divided the results by the mean impact velocity for a given fly-by, which results in mean number densities (in m$^{-3}$) in various bins. Vertical error bars reflect statistical errors due to the small number of impacts. The solid curve is the theoretical distribution of the impact ejecta expected for interplanetary impactors with a plausible set of model parameters[10,14,15].

in Ganymede's debris cloud: a steady-state value of roughly ten tons with a factor of 10 uncertainty.

The solid curve in Fig. 3 shows the predictions of an impact ejecta model[10,14,15], in which the interplanetary dust particles strike the surface of Ganymede, ejecting secondary particles. After choosing plausible values for the flux of interplanetary micrometeroids and the physical properties of Ganymede's surface, we find that the model predictions fit the dust data reasonably well. Our measurements and dynamical modelling therefore strongly suggest that the dusty debris near Ganymede is produced by a continuous hail of interplanetary particles which strike this moon with enough energy to accelerate dusty debris off its surface. Similar clouds probably surround Europa and Callisto, and, indeed, any moon that lacks a gaseous atmosphere. The few previous attempts to directly detect dust close to satellites, most notably near the Moon[16], have led to inconclusive results. Our successful detection of dust in the vicinity of the large jovian satellites underscores the general nature of the process, and provides strong support that our own Moon is a source of dust in near-terrestrial space.

A tiny fraction of impact debris is ejected at speeds sufficient to escape from Ganymede entirely. This material goes into orbit around Jupiter and will eventually be swept up by one of the galilean satellites—these grains are probably responsible for some of the impact events detected by the dust instrument in the inner jovian system[5,6]. Unfortunately, the ring of material formed by these grains escaping from Ganymede is far too tenuous to be detected optically. However, the fraction of debris escaping a satellite is a steeply decreasing function of satellite mass: so steep that despite their reduced cross-sections, small moons may be better sources of dust than large moons[17]. This most clearly exemplified in the images of the jovian ring provided by Galileo. These images show that the two tiny innermost moons, Adrastea and Metis, are sources for the main jovian ring and dusty halo, while Thebe and Amalthea each give rise to a faint outer gossamer ring of dusty material[18,19]. Medium-sized moons can also produce detectable rings: at Saturn the moon Enceladus supplies material to the broad and tenuous E ring[20] which, nevertheless, is substantial enough to be visible to ground-based telescopes. Impact ejection of dusty debris is likely to be important for explaining the distinctive black–white asymmetry of Saturn's moon Iapetus[21], for transporting exogenous material to Titan[21,22], and for producing dust in the uranian[23] and neptunian ring systems[24].

Future spacecraft measurements near planetary satellites are expected to quantify this important dust-production mechanism, and provide critical insight into the impact genesis of dusty rings. The next spacecraft likely to make *in situ* measurements of impact-generated grains is Nozomi (formerly called Planet-B). It will attempt to detect dust belts around Mars, which are predicted to originate from impacts onto Phobos and Deimos[25,26]. In mid-2004, the Cassini spacecraft should arrive at Saturn. Cassini, which is equipped with an improved version of the Galileo dust instrument, is intended to make numerous passes near the saturanian satellites and will fly through the tenuous E ring, thereby sampling both the bound and escaping components of Enceladus ejecta. □

Received 12 February; accepted 15 April 1999.


1. Grün, E. *et al*. The Galileo dust detector. *Space Sci. Rev.* **60,** 317–340 (1992).
2. Grün, E. *et al*. The Ulysses dust experiment. *Astron. Astrophys. Suppl. Ser.* **92,** 411–423 (1992).
3. Grün, E. *et al*. Reduction of Galileo and Ulysses dust data. *Planet. Space Sci.* **43,** 941–951 (1995).
4. Krüger, H. *et al*. Three years of Galileo dust data: II. 1993 to 1995. *Planet. Space Sci.* **47,** 85–106 (1999).
5. Grün, E. *et al*. Dust measurements in the jovian magnetosphere. *Geophys. Res. Lett.* **24,** 2171–2174 (1997).
6. Grün, E. *et al*. Galileo observes electromagnetically coupled dust in the jovian magnetosphere. *J. Geophys. Res.* **103,** 20011–20022 (1998).
7. Krüger, H., Grün, E., Graps, A. & Lammers, S. Observations of electromagnetically coupled dust in the Jovian magnetosphere. *Astrophys. Space Sci.* (in the press).
8. Grün, E. *et al*. Discovery of jovian dust streams and interstellar grains by the Ulysses spacecraft. *Nature* **362,** 428–430 (1993).
9. Grün, E. *et al*. Constraints from Galileo observations on the origin of jovian dust streams. *Nature* **381,** 395–398 (1996).
10. Krüger, H., Krivov, A. V., Grün, E. & Hamilton, D. P. A dust cloud of Ganymede maintained by hypervelocity impacts of micrometeroids. *J. Geophys. Res.* (submitted).
11. Zook, H. A. *et al*. Solar wind magnetic field bending of jovian dust trajectories. *Science* **274,** 1501–1503 (1996).
12. Koschny, D. & Grün, E. Impacts into ice-silicate mixtures: Crater morphologies, volumes, depth-to-diameter ratios and yield. *Icarus* (submitted).
13. Koschny, D. & Grün, E. Impacts into ice-silicate mixtures: Ejecta mass and size distributions. *Icarus* (submitted).
14. Krivov, A. V. On the dust belts of Mars. *Astron. Astrophys.* **291,** 657–663 (1994).
15. Krivov, A. V. & Jurewicz, A. The ethereal dust envelopes of the Martian moons. *Planet. Space Sci.* **47,** 45–56 (1999).
16. Iglseder, H., Uesugi, K. & Svedhem, H. Cosmic dust measurements in lunar orbit. *Adv. Space Res.* **17,** 177–182 (1996).
17. Burns, J. A., Showalter, M. R. & Morfill, G. E. in *Planetary Rings* (eds Greenberg, R. & Brahic, A.) 200–272 (Univ. Arizona Press, Tucson, 1984).
18. Ockert-Bell, M. E. *et al*. The structure of Jupiter's ring system as revealed by the Galileo imaging experiment. *Icarus* **138,** 188–219 (1999).
19. Burns, J. A. *et al*. The formation of Jupiter's faint rings. *Science* **284,** 1146–1150 (1999).
20. Hamilton, D. P. & Burns, J. A. Origin of Saturn's E ring: self-sustained, naturally. *Science* **264,** 550–553 (1994).
21. Burns, J., Hamilton, D. P., Mignard, F. & Soter, S. in *Physics, Chemistry, and Dynamics of Interplanetary Dust* (eds Gustafson, B. A. S. & Hanner, M. S.) 179–182 (Vol. 104, ASP Conf. Ser., Kluwer, Dordrecht, 1996).
22. Banaszkiewicz, M. & Krivov, A. V. Hyperion as a dust source in the saturnian system. *Icarus* **129,** 289–303 (1997).
23. Esposito, L. W., Brahic, A., Burns, J. A. & Marouf, E. A. in *Uranus* (eds Bergstrahl, J. T., Miner, E. A. & Matthews, M. S.) 410–465 (Univ. Arizona Press, Tucson, 1991).
24. Colwell, J. E. & Esposito, L. W. A model of dust production in the Neptune ring system. *Geophys. Res. Lett.* **17,** 1741–1744 (1990).
25. Soter, S. *The Dust Belts of Mars* (Report of Center for Radiophysics and Space Research No. 462, 1971).
26. Krivov, A. V. & Hamilton, D. P. Martian dust belts: Waiting for discovery. *Icarus* **128,** 335–353 (1997).


**Acknowledgements.** We thank the Galileo project at JPL for effective and successful mission operations. A.K. thanks his colleagues in the Heidelberg dust group for their hospitality and for funding his stay at MPIK. This work was supported by Deutsches Zentrum für Luft- und Raumfahrt e.V. (DLR).

Correspondence and requests for materials should be addressed to H.K. (e-mail: krueger@galileo.mpi-hd.mpg.de).

# Percolative phase separation underlies colossal magnetoresistance in mixed-valent manganites

**M. Uehara*†, S. Mori‡†, C. H. Chen‡ & S.-W. Cheong*‡**

** Department of Physics and Astronomy, Rutgers University, Piscataway, New Jersey 08854, USA*

*† Bell Laboratories, Lucent Technologies, Murray Hill, New Jersey 07974, USA*

**Colossal magnetoresistance[1]—an unusually large change of resistivity observed in certain materials following application of magnetic field—has been extensively researched in ferromagnetic perovskite manganites. But it remains unclear why the magnetoresistive response increases dramatically when the Curie temperature ($T_C$) is reduced. In these materials, $T_C$ varies sensitively with changing chemical pressure; this can be achieved by introducing trivalent rare-earth ions of differing size into the perovskite structure[2–4], without affecting the valency of the Mn ions. The chemical pressure modifies local structural parameters such as the Mn–O bond distance and Mn–O–Mn bond angle, which directly influence the case of electron hopping between Mn ions (that is, the electronic bandwidth). But these effects cannot satisfactorily explain the dependence of magnetoresistance on $T_C$. Here we demonstrate, using electron microscopy data, that the prototypical (La,Pr,Ca)$MnO_3$ system is electronically phase-separated into a sub-micrometre-scale mixture of insulating regions (with a particular type of charge-ordering) and metallic, ferromagnetic domains. We find that the colossal magnetoresistive effect in low-$T_C$ systems can be explained by percolative transport through the ferromagnetic domains; this depends sensitively on the rela-**

† Permanent addresses: Department of Physics, Aoyama-Gakuin University, Tokyo 157-8572, Japan (M.U.); Department of Physics, Tokyo Institute of Technology, Tokyo 152-8551, Japan (S.M.).